Electronic Supplementary Material (ESI) for ChemComm.

Supporting Information

Blue-emitting pyrene-based aggregates

Jorge S. Valera,[a] Joaquín Calbo,[b] Rafael Gómez,[a] Enrique Ortí*[b] and Luis Sánchez*[a]

[a] *Departamento de Química Orgánica, Facultad de Ciencias Químicas, Universidad Complutense de Madrid, 28040 Madrid (Spain). E-mail: lusamar@quim.ucm.es*

[b] *Instituto de Ciencia Molecular, Universidad de Valencia, 46980 Paterna (Spain); E-mail: enrique.orti@uv.es*

Contents:

1. Supplementary Figures and Tables

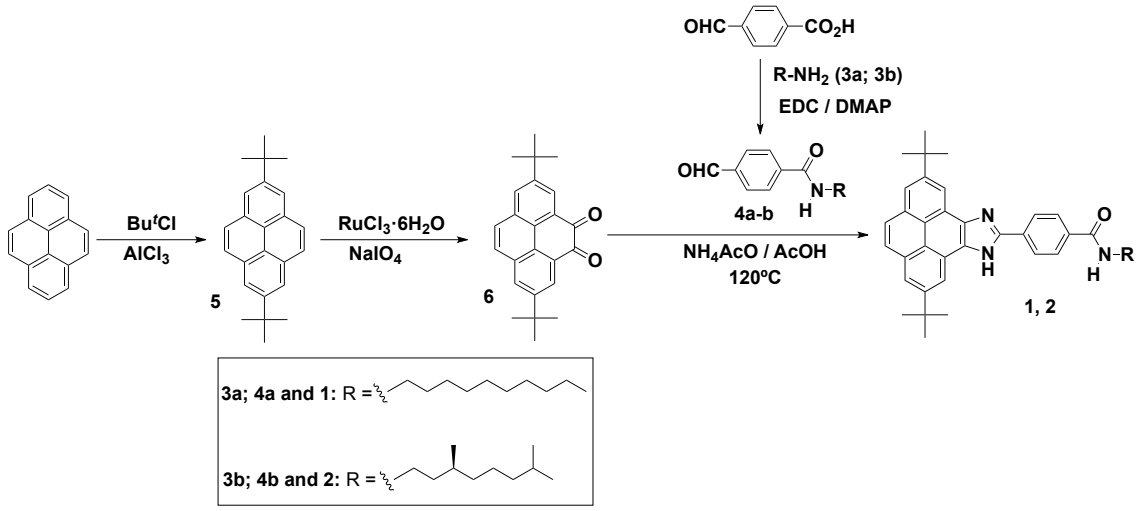

Scheme S1. Synthesis of pyreneimidazoles **1** and **2**.

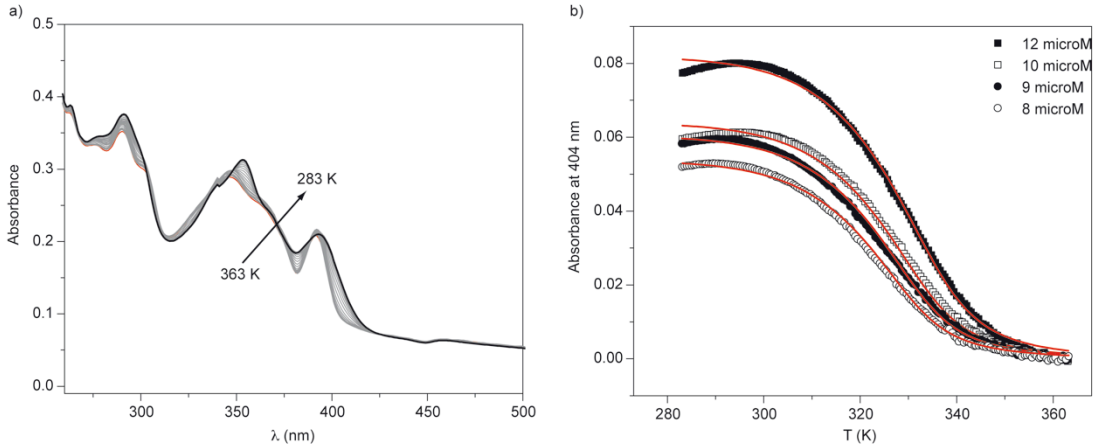

Figure S1. (a) Variable temperature UV-Vis spectra of **1** at 8×10^{-6} M in MCH. (b) UV-Vis cooling curves of compound **1** (MCH, measured at λ = 404 nm). Red lines correspond to the fitting to the EQ model.

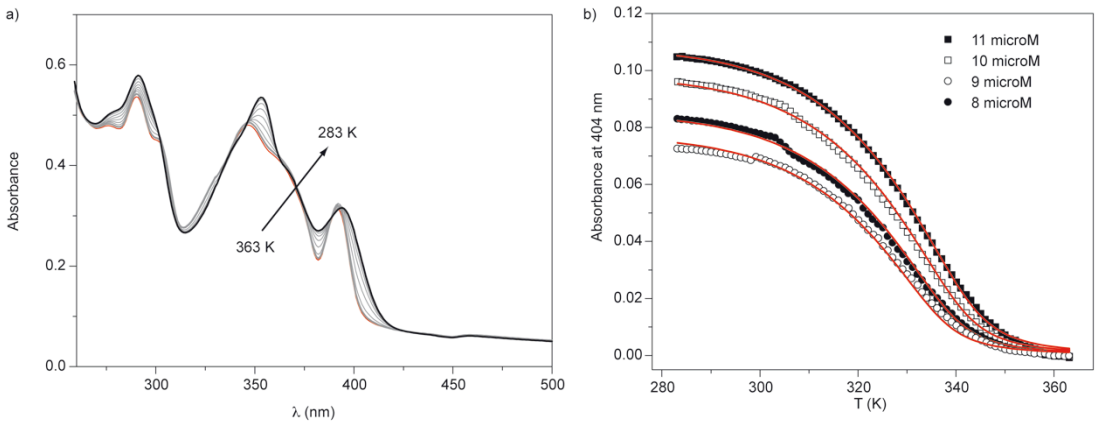

Figure S2. (a) Variable temperature UV-Vis spectra of **2** at 1×10^{-5} M in MCH. (b) UV-Vis cooling curves of compound **2** (MCH, measured at λ = 404 nm). Red lines correspond to the fitting to the EQ model.

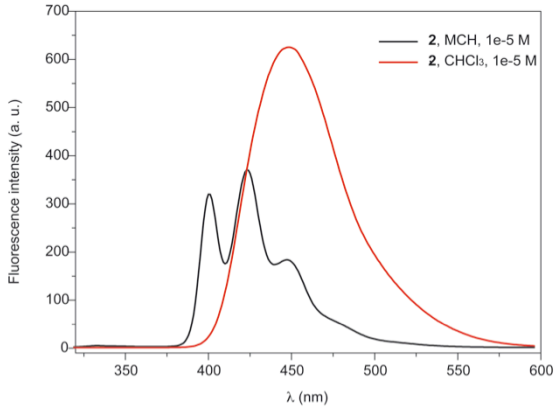

Figure S3. Emission spectra of **2** in MCH and $CHCl_3$ (298 K, 1×10^{-5} M, λ_{exc} = 334 nm).

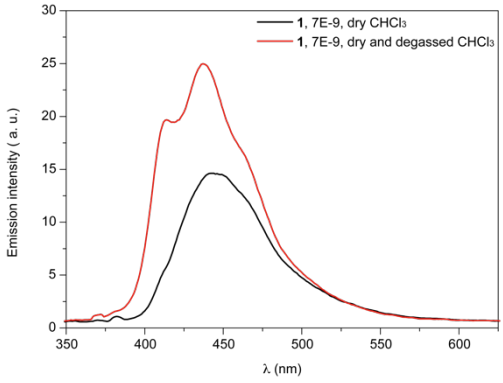

Figure S4. Emission spectra of **1** in $CHCl_3$ at different experimental conditions (298 K, 7×10^{-9} M, λ_{exc} = 334 nm).

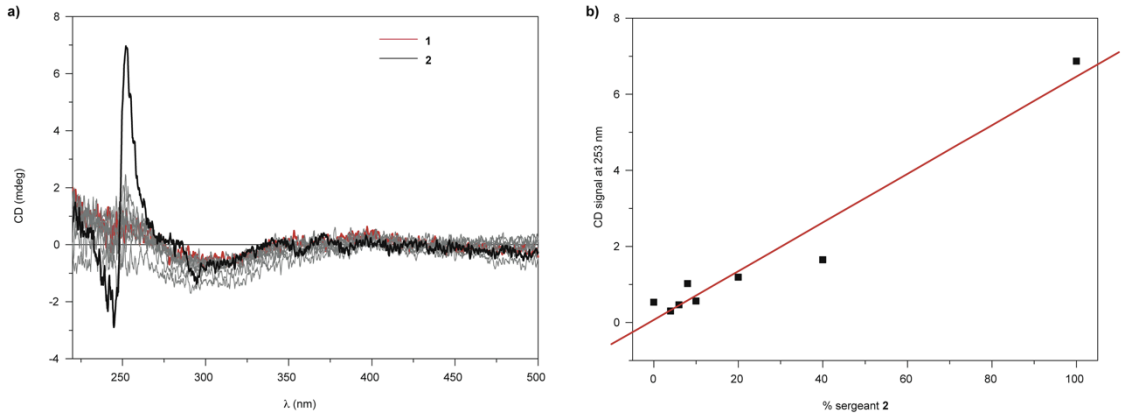

Figure S5. Sergeants-and-soldiers (SaS) experiments for achiral **1** upon mixing with chiral **2** (298 K, MCH, total concentration, 1×10^{-5} M). Panel (a) depicts the CD spectra and panel (b) depicts the linear variation of the CD response at 253 nm upon increasing the amount of the chiral sergeant **2**.

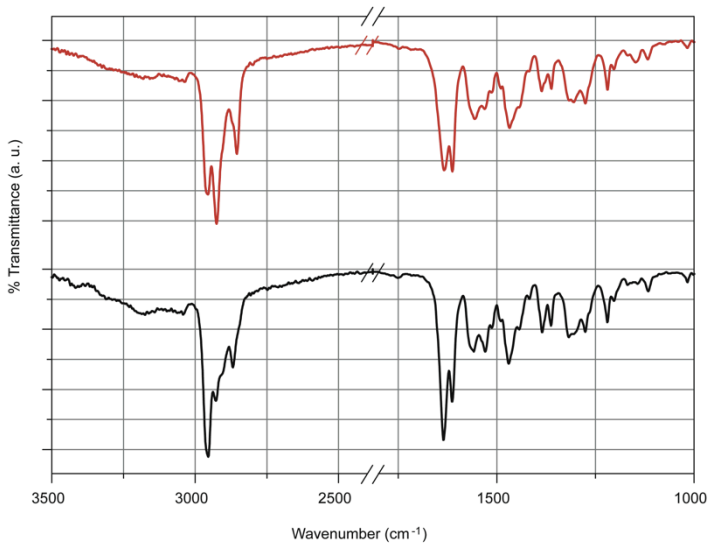

Figure S6. Partial FTIR spectra (neat) of pyreneimidazoles **1** (top) and **2** (bottom).

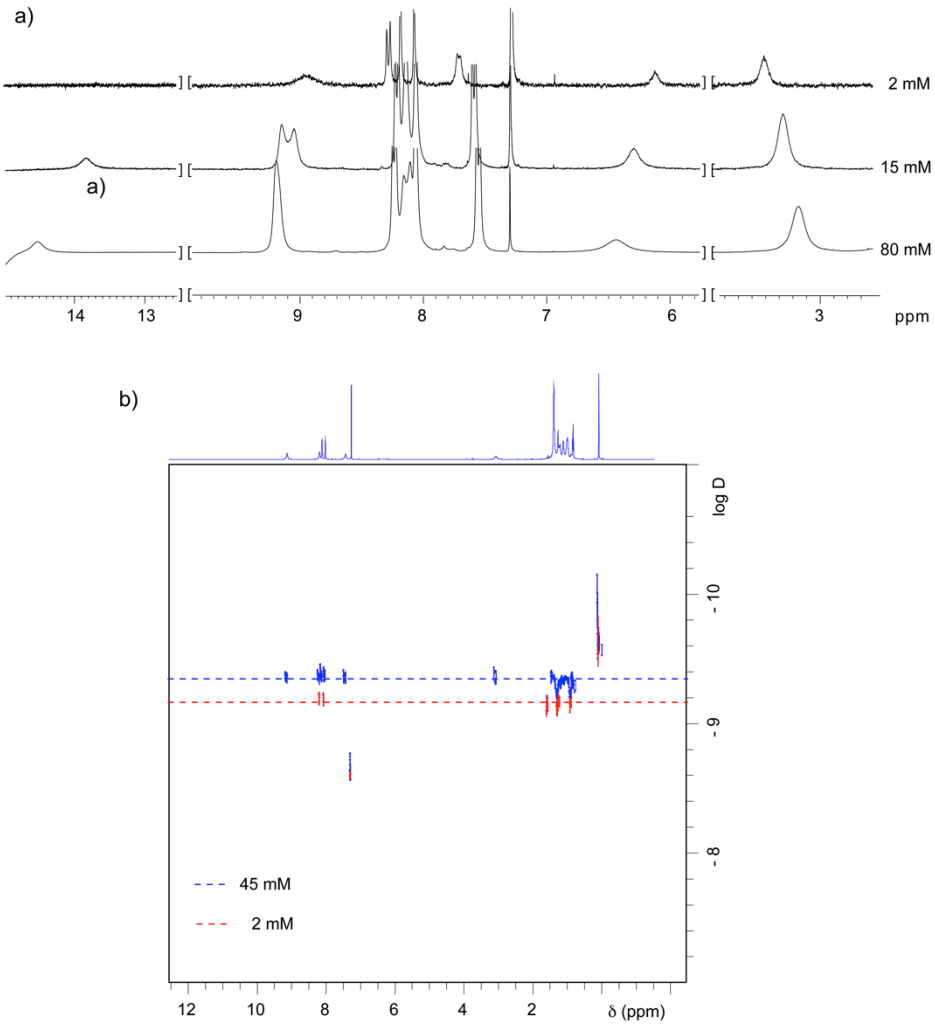

Figure S7. Partial ^{1}NMR (a) and ^{1}H DOSY NMR (Δ = 160 ms, t = 3 ms) (b) spectra of **1** at different concentrations ($CDCl_3$, 298 K, 300 MHz).

2. Theoretical calculations

Theoretical calculations were performed within the density functional theory (DFT) framework. All the calculations were performed by using the Gaussian 09 (revision D01) suite of programs.[1] We first modelled compound **1** by replacing the aliphatic decyl chain by a hydrogen atom to reduce the computational cost (Figure S8a). The Grimme's B97D functional,[2] which includes dispersion corrections, was employed in combination with the split-valence, double-zeta quality 6-31G** basis.[3-5] The B97D/6-31G** minimum-energy geometry calculated for **1** is disposed in a coplanar fashion in which the imidazole and the benzene rings remain in the plane of the pyrene core. The amide group was first modelled to be coplanar with the adjacent benzene ring resulting in a geometry with C_s symmetry. However, by eliminating any symmetry constraint, the amide group adopts an out-of-plane arrangement (θ = 18.5°) with respect to the benzene plane in order to reduce the steric hindrance provoked by short Ar–H···H–N contacts (Figure S8a). The twisted conformation (C_1 symmetry) is 0.66 kcal/mol more stable than the C_s conformer and the distance *d* lengthens from 2.03 to 2.19 Å. The out-of-plane disposition of the amide in the C_1 conformer facilitates a columnar stacking growth led by amide–amide H-bond interactions. After inclusion of the aliphatic chain (Figure S8b), the amide twisting angle increases to 23.8° and the distance *d* is kept at 2.13 Å.

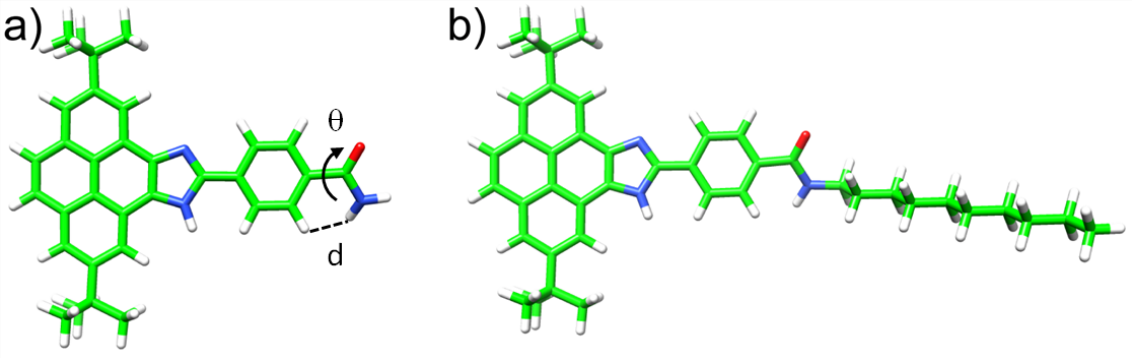

Figure S8. a) Pyreneimidazole system simplified by eliminating the aliphatic chain. b) B97D/6-31G** minimum-energy geometry calculated for compound **1**.

Figure S9 displays the molecular electrostatic potential (MEP) calculated for **1** using Becke's 3-parameter Lee-Yang-Parr hybrid functional (B3LYP)[6] together with the 6-31G** basis set. The MEP surface shows that the largest potential energy values are located over the amide and imidazole groups. Negative potential energies of –55.7 and –54.6 kcal/mol are calculated in the oxygen and nitrogen vicinity, whereas positive

potentials of +101.2 and +121.0 kcal/mol are located over the N–H region of the amide and imidazole. The benzene and pyrene π-holes have potential energies of +29.1 and +31.6 kcal/mol, respectively. Strong electrostatic interactions between monomers are then expected in the amide and imidazole vicinity, whereas π-π and C-H···π dispersion interactions may be achieved in the pyrene, benzene and aliphatic chain regions.

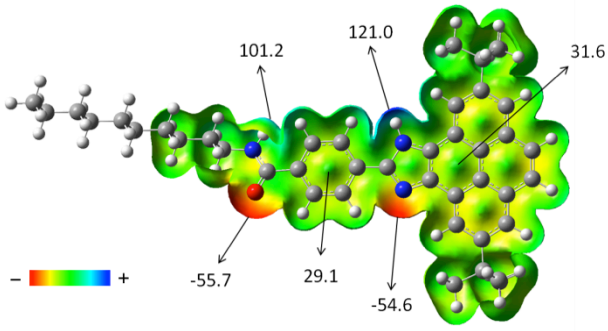

Figure S9. B3LYP/6-31G** molecular electrostatic potential surface mapped onto the electron density isosurface with isovalue = 0.01 a.u. The surface was cut parallel to the viewing plane. Potential energies (in kcal/mol) are indicated for relevant points on the surface.

A large number of dimers were modelled in order to rationalize how the pyreneimidazole compound **1** supramolecularly aggregates (Figure 4 in the main text). The geometry optimization of all the dimers was performed by means of the Grimme's B97 functional including the most recent D3 dispersion correction using the Becke-Johnson damping function (B97D3).[7] The double-zeta 6-31G** basis set was employed. No counterpoise correction was applied to correct the basis set superposition error (BSSE). Note that the counterpoise method is believed to overestimate the BSSE, for which some authors propose to scale it down by half of its value.[8]

Non-covalent interaction (NCI) plots were computed for the optimized geometries of dimers **A–F** at the B97D3/6-31G** level using the NCIPLOT program.[9,10] The method used for the NCI analysis is based on the relationship between the reduced density gradient (RDG) and the electron density (ρ). The molecular electron density computed from the sum of atomic contributions, the so-called promolecular density, was employed as an approach to ρ. The density and RDG cutoffs were kept at their default values. Figure S10 shows the NCI surfaces calculated for all the dimers modelled for **1**. Green regions refer to weak dispersion-based interactions, whereas blue contours indicate H-bonding interactions.

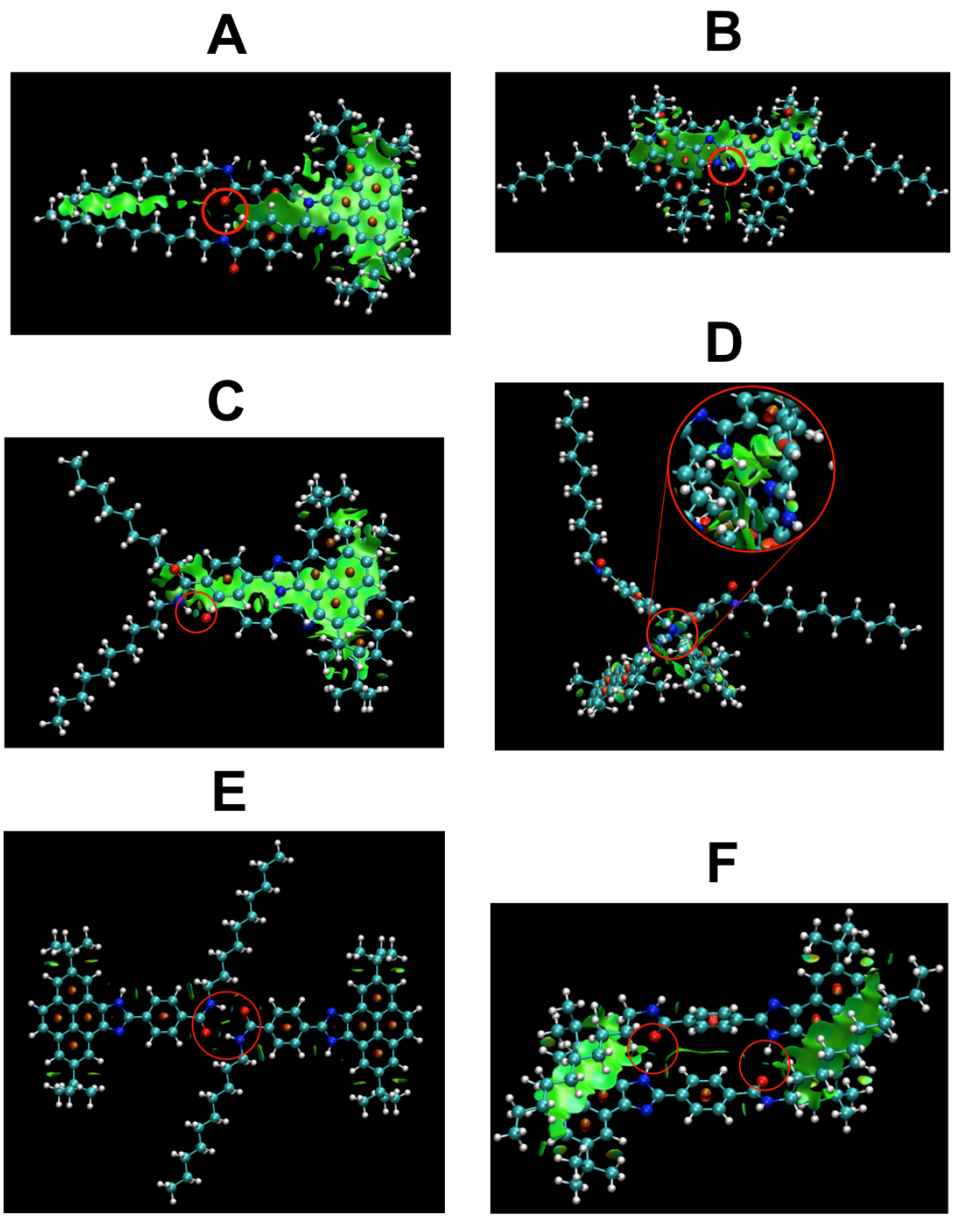

Figure S10. NCI surfaces representing H-bond interactions (in blue and surrounded by red circles) and dispersion forces (in green) for dimers **A–F** of compound **1**. Intramolecular ring-centroid repulsions are drawn in dark red.

Figure S11 displays the RDG plots for all the dimers. The positive peaks close to RDG = 0 at ρ = 0.05 and 0.10 correspond to repulsive ring-centre interactions, whereas negative peaks at $-0.06 < \rho < -0.02$ indicate the presence of H-bond contacts. Peaks close to the ρ = 0 region are associated to dispersion forces. By comparing the different RDG plots, the main differences are obtained for dimer **E**, which does not show low values of RDG at $\rho \sim 0$ indicating the absence of intermolecular dispersion interactions. The sharp peaks computed close to ρ = –0.05 in dimers **D**, **E** and **F** are indicative of strong H-bond contacts.

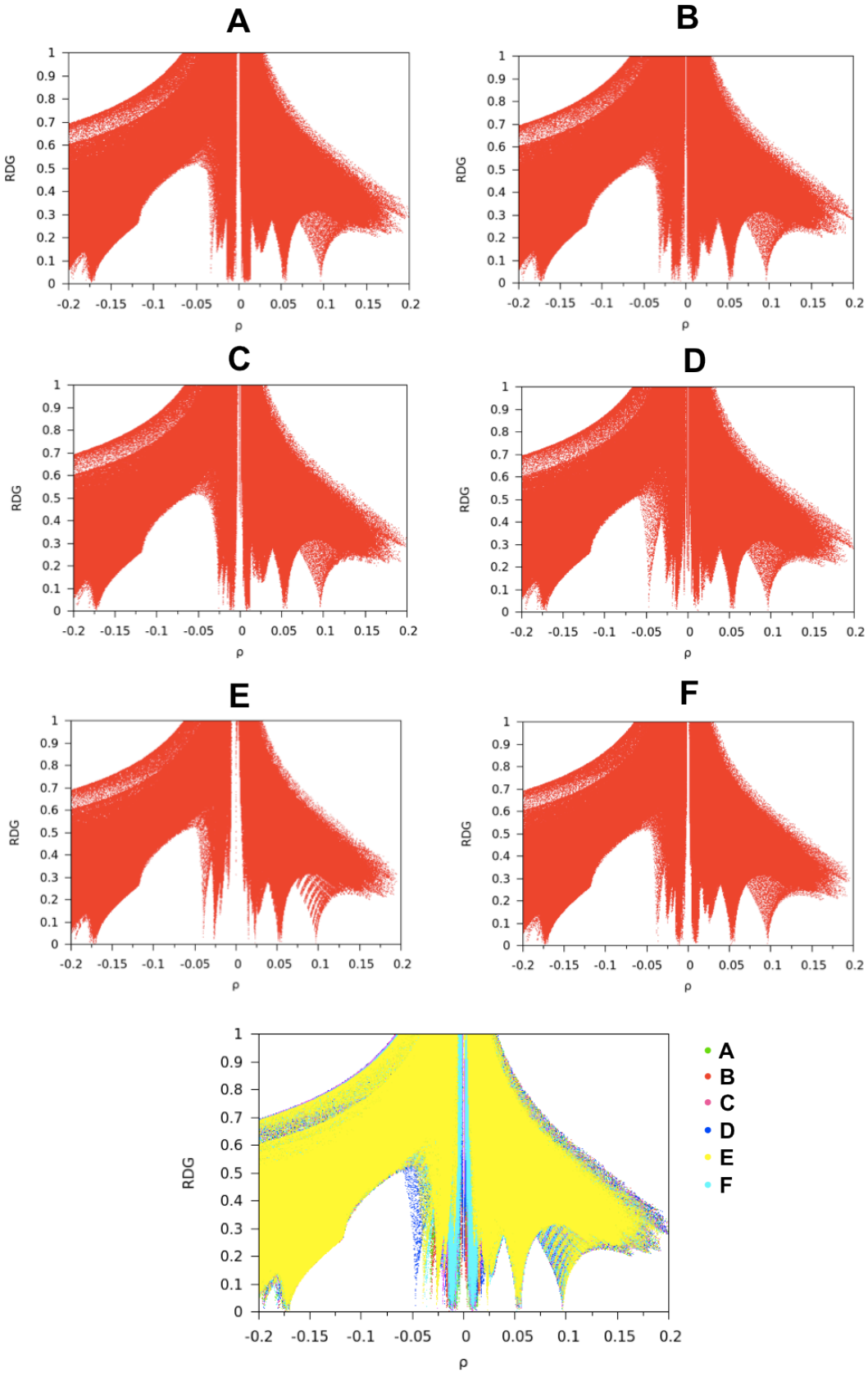

Figure S11. Reduced density gradient (RDG) behavior for dimers **A–F** of compound **1**. The combination of all the RDG plots in one is shown in the last graph.

The tetramer modelled for the **F**-type aggregation mode (Figure 5 in the main text) was fully optimized at the B97D3/6-31G** level of theory. The interaction energy between monomer pairs in the tetramer was calculated at the same level of theory.

N-propylbenzamide was used as a simplified model to estimate the energy required to pass from a *trans*- to a *cis*-like amide (Figure S12). Whereas the alkyl chain has a large degree of freedom to adopt the optimal disposition (a flat potential energy profile is computed for the C–N–C–C dihedral angle between the two minima at 90 and 270°; Figure S12b), a large barrier of 15 kcal/mol is computed to convert a *trans*-amide into a *cis* conformation (Figure S12a).

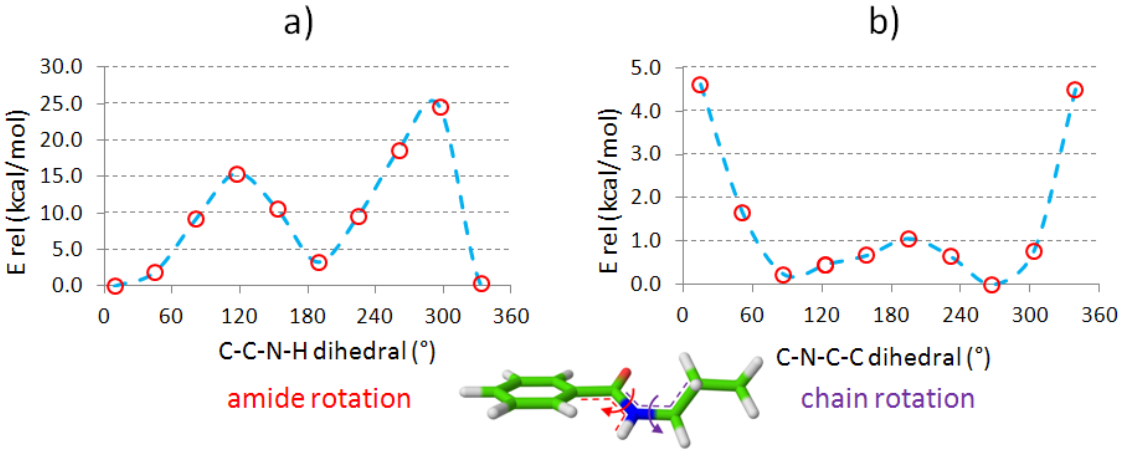

Figure S12. Optimized torsional potentials (E_{rel}) computed for: a) the amide C–C–N–H dihedral angle that interconverts the *trans* (0 and 360°) into the *cis* (180°) conformer, and b) the dihedral C–N–C–C angle between the amide group and the alkyl chain.

Chemical structures were modeled by using the Chemcraft 1.7 software.[11] The MEP surface was depicted by means of Gaussview 5.0.[12] The NCI surfaces were created in the VMD (version 1.8.3) program.[13] The GNUPLOT 4.6 was utilized to plot the RDG graphs.[14]

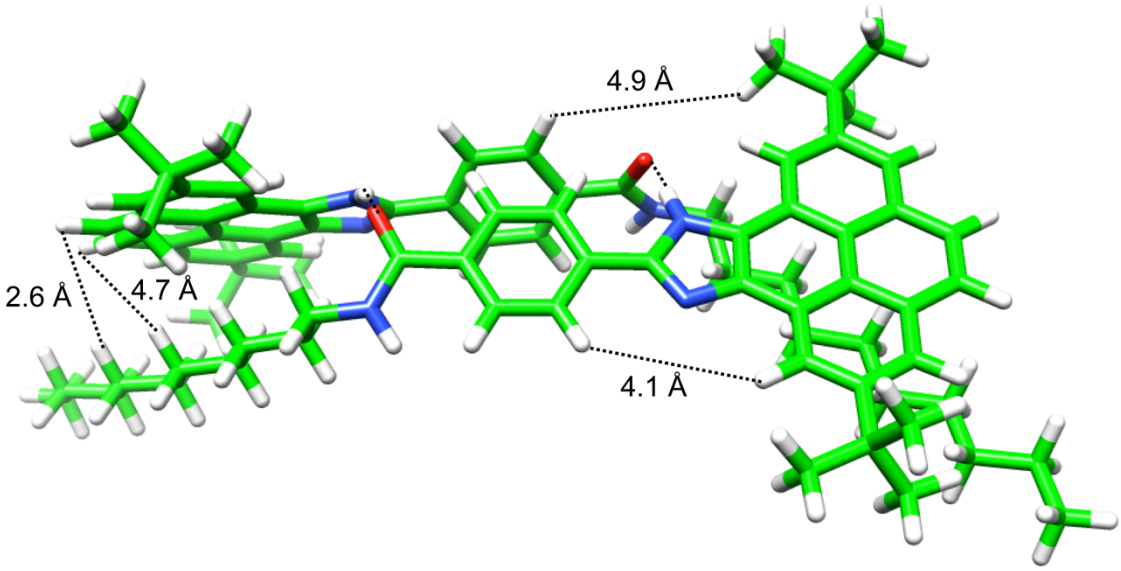

Figure S13. Minimum-energy geometry calculated for dimer **F** showing selected through-space distances observed in the ROESY experiment.

3. Experimental section

General. All solvents were dried according to standard procedures. Reagents were used as purchased. All air-sensitive reactions were carried out under argon atmosphere. NMR spectra were recorded on a Bruker Avance 300 (^{1}H: 300 MHz; ^{13}C: 75 MHz) spectrometer at 298 K using partially deuterated solvents as internal standards. Coupling constants (J) are denoted in Hz and chemical shifts (δ) in ppm. Multiplicities are denoted as follows: s = singlet, d = doublet, t = triplet, m = multiplet, br = broad. ^{1}H NMR spectroscopic diffusion measurements (DOSY) were performed using a stimulated echo sequence with bipolar gradient pulses (BPLED) and were evaluated using Top Spin 2.1 software. Diffusion time was set within the range 50-150 ms. Pulsed gradients were incremented from 2 to 95 % of the maximum strength in sixteen-spaced steps with a duration of 2.6 to 4 ms. The amplitude of the pulsed-field gradients was calibrated using the known ^{1}H diffusion coefficient in D_2O D= $1.90.10^{-9}$ m^2 s^{-1}. Data were acquired without sample rotation and the temperature was controlled at 298 K to minimize convection effects. FT-IR spectra were recorded on a Bruker Tensor 27 (ATR device) spectrometer. UV-Vis spectra were recorded on a Varian Cary 50 spectrophotometer. High resolution mass spectra (HRMS) were recorded on a FTMS Bruker APEX Q IV spectrometer. UV-Vis spectra were registered on a Jasco-V630 spectrophotometer equipped with a Peltier thermoelectric temperature controller. The spectra were recorded in the continuous mode between 200 and 800 nm, with a wavelength increment of 1 nm, a response time of 4 s, and a bandwidth of 1 nm. A 1 mm path length quartz cuvette (Hellma) was used. Thermal experiments were performed at constant heating rates of 1 K min^{-1} in methylcyclohexane. Circular dichroism (CD) measurements were performed on a Jasco-810 dichrograph equipped with a Peltier thermoelectric temperature controller. The spectra were recorded in the continuous mode between 400 and 200 nm, with a wavelength increment of 1 nm, a response time of 4 s, and a bandwidth of 1 nm. A 1 cm path length quartz cuvette (Hellma) was used. Spectra from three scans were averaged. Fluorescence spectra were recorded on a Jasco FP-6500 spectrophotometer.

4. Synthetic details and characterization

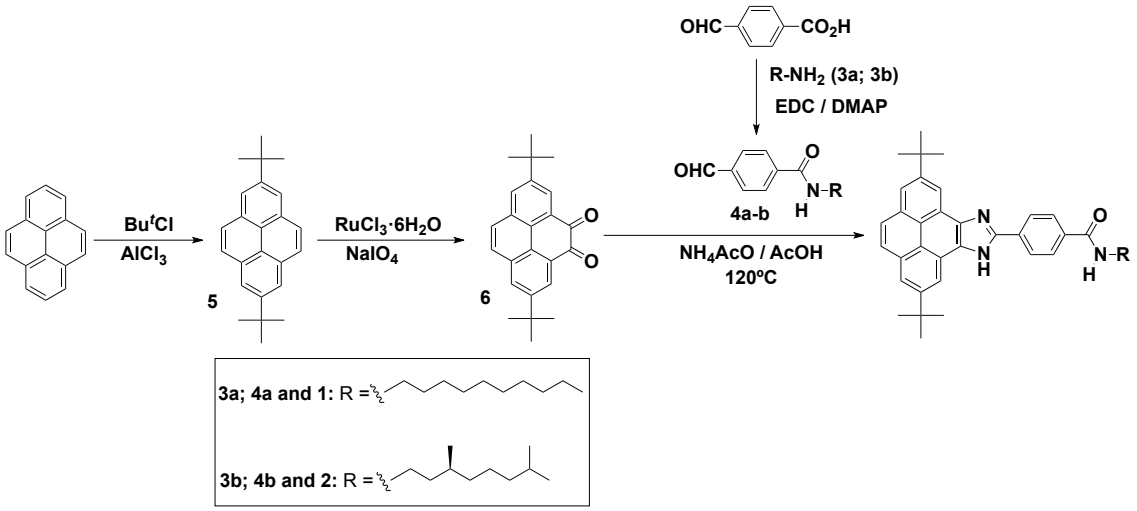

Amine **3b** and 2,7-di-*tert*-butyl-4,5-pyrenedione (**6**) were prepared according to previously reported synthetic procedures and showed identical spectroscopic properties to those reported therein.[15,16]

***N*-decyl-4-formylbenzamide (4a).**

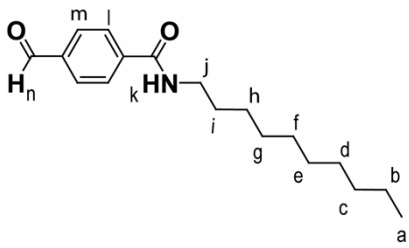

EDC (2.81 g, 14.65 mmol) and DMAP (1.80 g, 14.65 mmol) are added to a solution of 4-formylbenzoic acid (2.00 g, 13.32 mmol) in 20 mL of CH_2Cl_2 at 0 °C, under argon atmosphere. After 15 minutes, n-decylamine (2.8 mL, 13.32 mmol) is added dropwise and the resulting mixture is stirred at room temperature overnight. After that, the reaction mixture is washed with HCl, NaOH and brine. The organic layer is dried with $MgSO_4$ and the solvent removed in vacuo. The afforded crude is subjected to silica column chromatography ($CHCl_3$/MeOH 10:0.3 as eluent) to give product **4a** as a white solid (2.02 g, 6.97 mmol). Yield: 52 %. ^{1}H NMR (300 MHz, $CDCl_3$) (δ / ppm): 0.88 (t, $3H_a$, J = 7.0 Hz), 1.27-1.70 (br, 16 $H_{b+c+d+e+f+g+h+i}$), 3.49 (br, $2H_j$), 6.22 (br, $1H_k$), 7.91 (d, $2H_l$, J = 8.9 Hz), 7.95 (d, $2H_m$, J = 8.9 Hz), 10.08 (s, $1H_n$). ^{13}C NMR (75 MHz, $CDCl_3$) (δ / ppm): 14.2, 22.8, 27.1, 29.4, 29.7, 32.0, 40.5, 127.7, 130.0, 138.3, 140.2, 166.5, 191.6. FTIR ($\hat{u}$ / cm^{-1}): 623, 637, 757, 819, 847, 1206, 1308, 1322, 1322, 1474, 1500, 1536, 1610, 1629, 1696, 1707, 2850, 2922, 2955, 3331. EI-MS: $C_{18}H_{27}NO_2$ $[M]^+$, 289.20.

(*S*)-*N*-(3,7-dimethyloctyl)-4-formylbenzamide (4b).

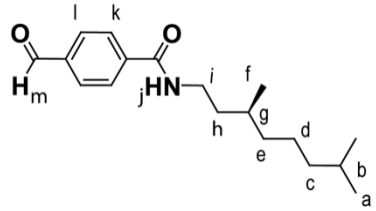

EDC (1.22 g, 6.36 mmol) and DMAP (0.78 g, 6.36 mmol) are added to a solution of 4-formylbenzoic acid (0.87 g, 5.78 mmol) in 15 mL of CH_2Cl_2 at 0 °C, under argon atmosphere. After 15 minutes, (*S*)-3,7-dimethyloctan-1-amine **3b** (1.00 g, 6.36 mmol) is added dropwise and the resulting mixture is stirred at room temperature overnight. After that, the reaction mixture is washed with HCl, NaOH and brine. The organic layer is dried with $MgSO_4$ and the solvent removed in vacuo. The afforded crude is subjected to silica column chromatography ($CHCl_3$/MeOH 10:0.3 as eluent) to give product **4b** as a white solid (0.66 g, 2.28 mmol). Yield: 40 %. ^{1}H NMR (300 MHz, $CDCl_3$) (δ / ppm): 0.80 (d, 6H$_a$, J = 6.6 Hz), 0.87 (3H$_g$, J = 6.6 Hz), 1.04-1.72 (br, 10H$_{b+c+d+e+f+h}$), 3.44 (m, 2H$_i$), 6.76 (t,1H$_j$, J = 4.9 Hz), 7.84 (d, 2H$_k$, J = 8.8 Hz), 7.89 (d, 2H$_l$, J = 8.8 Hz), 9.99 (s, 1H$_m$). ^{13}C NMR (75 MHz, $CDCl_3$) (δ / ppm): 19.7, 22.7, 22.8, 24.8, 28.1, 30.9, 36.8, 37.2, 38.6, 39.3, 127.7, 130.0, 138.2, 140.2, 166.5, 191.7. FTIR ($\hat{u}$ / cm^{-1}): 628, 671, 758, 821, 849, 1013, 1106, 1151, 1206, 1314, 1381, 1464, 1501, 1541, 1636, 1704, 2867, 2925, 2956, 3075, 3312. EI-MS: $C_{18}H_{27}NO_2$ [M]$^+$, 289.20.

4-(2,7-di-*tert*-butyl-9H-pyrene[4,5-d]imidazole-10-yl)-*N*-decylbenzamide (1).

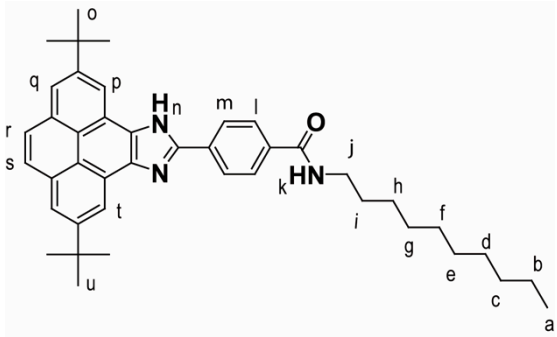

Aldehyde **4a** (0.12 g, 0.4 mmol) and ammonium acetate (0.15 g, 2 mmol) are added to a solution of 2,7-di-*tert*-butyl-4,5-pyrenedione **6** (0.14 g, 0.4 mmol) in 5 mL of acetic acid. The resulting mixture is heated under reflux overnight. After that, the reaction mixture is quenched with 30 mL of water to afford a precipitate, which is subsequently dissolved in CH_2Cl_2. The resulting solution is dried with $MgSO_4$ and the solvent removed in vacuo, affording a crude that is subjected to silica gel column chromatography (CH_2Cl_2/MeOH 10:0.1 as eluent) to give product **1** as a yellow solid (0.14 g, 0.21 mmol). Yield: 56 %. ^{1}H NMR (700 MHz, DMSO – d6) (δ / ppm): 0.85 (t, 3H$_a$, J = 7.0 Hz), 1.20-

1.37 (br, 16$H_{b+c+d+e+f+g+h+i}$), 1.60 (s, 9$H_{o\ or\ u}$), 1.62 (s, 9$H_{u\ or\ o}$), 3.30 (br, 2H_j), 8.10 (d, 2H_l, J = 8.2 Hz), 8.14 (d, 1$H_{r\ or\ s}$, J = 8.9 Hz), 8.16 (d, 1$H_{s\ or\ r}$, J = 8.9 Hz), 8.26 (d, 2H_q, J = 1.2 Hz), 8.45 (d, 2H_m, J = 8.2 Hz), 8.62 (t, 1H_k, J = 5.8 Hz), 8.84 (d, 1$H_{p\ or\ t}$, J = 1.2 Hz), 8.91 (d, 1$H_{t\ or\ p}$, J = 1.2 Hz), 13.72 (s, 1H_n). ^{13}C NMR (176 MHz, DMSO – d6) (δ / ppm): 14.0, 22.1, 26.6, 28.7, 28.8, 29.0, 29.1, 29.2, 31.3, 31.8, 35.1, 35.3, 115.9, 116.5, 120.1, 120.2, 121.1, 121.2, 125.7, 125.9, 127.6, 127.9, 128.0, 128.8, 131.2, 131.3, 132.6, 134.9, 137.9, 148.2, 148.6, 148.7, 165.5. FTIR ($\tilde{\upsilon}$ / cm^{-1}): 725, 858, 879, 1220, 1276, 1306, 1362, 1386, 1467, 1531, 1556, 1613, 1633, 2854, 2925, 2965. HRMS (ESI-FT) calcd. for $C_{42}H_{51}N_3O$ [M]$^+$, 613.4027; found, 613.4029.

(*S*)-4-(2,7-di-*tert*-butyl-9H-pyrene[4,5-d]imidazole-10-yl)-*N*-(3,7-dimethyloctyl)-benzamide (2).

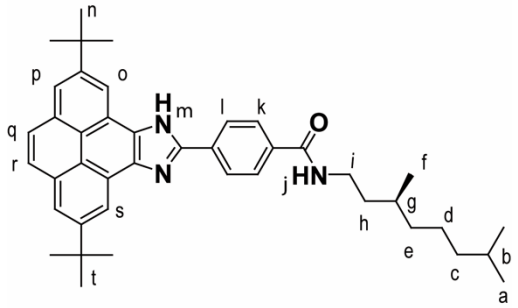

Aldehyde **4b** (0.17 g, 0.6 mmol) and ammonium acetate (0.23 g, 3 mmol) are added to a solution of 2,7-di-*tert*-butyl-4,5-pyrenedione **6** (0.21 g, 0.6 mmol) in 8 mL of acetic acid. The resulting mixture is heated under reflux overnight. After that, the reaction mixture is quenched with 40 mL of water to afford a precipitate which is subsequently dissolved in CH_2Cl_2. The resulting solution is dried with $MgSO_4$ and the solvent removed in vacuo, affording a crude that is subjected to silica gel column chromatography (CH_2Cl_2/MeOH 10:0.1 as eluent) to give product **2** as a yellow solid (0.23 g, 0.37 mmol). Yield: 62 %. ^{1}H NMR (300 MHz, DMSO – d6) (δ / ppm): 0.85 (t, 6H_a, J = 7.4 Hz), 0.92 (d, 3H_f, J = 7.4 Hz) 1.13-1.53 (br, 10$H_{b+c+d+e+g+h}$), 1.60 (s, 9$H_{n\ or\ t}$), 1.62 (s, 9$H_{t\ or\ n}$), 3.32 (br, 2H_i), 8.10 (d, 2H_k, J = 8.6 Hz), 8.14 (d, 2H_{q+r}, J = 1.0 Hz), 8.26 (d, 2H_p, J = 1.8 Hz), 8.45 (d, 2H_l, J = 8.6 Hz), 8.60 (t, 1H_j, J = 5.5 Hz), 8.84 (d, 1$H_{o\ or\ s}$, J = 2.0 Hz), 8.90 (d, 1$H_{s\ or\ o}$, J = 2.0 Hz), 13.71 (s, 1H_m). ^{13}C NMR (176 MHz, DMSO – d6) (δ / ppm): 19.6, 22.5, 22.6, 24.1, 27.4, 30.1, 31.8, 35.1, 35.3, 36.3, 36.7, 37.4, 38.8, 116.0, 116.6, 120.1, 120.2, 121.1, 121.3, 125.7, 125.9, 127.6, 127.9, 128.0, 128.8, 131.2, 131.3, 132.6, 134.9, 137.9, 148.2, 148.6, 148.7, 165.5. FTIR ($\tilde{\upsilon}$ / cm^{-1}): 725, 857, 879, 1220, 1276, 1318, 1363, 1385, 1470, 1529, 1559, 1613, 1635, 2869, 2928, 2954. HRMS (ESI-FT) calcd. for $C_{42}H_{51}N_3O$ [M]$^+$, 613.4027; found, 613.4022.

5.- Collection of spectra

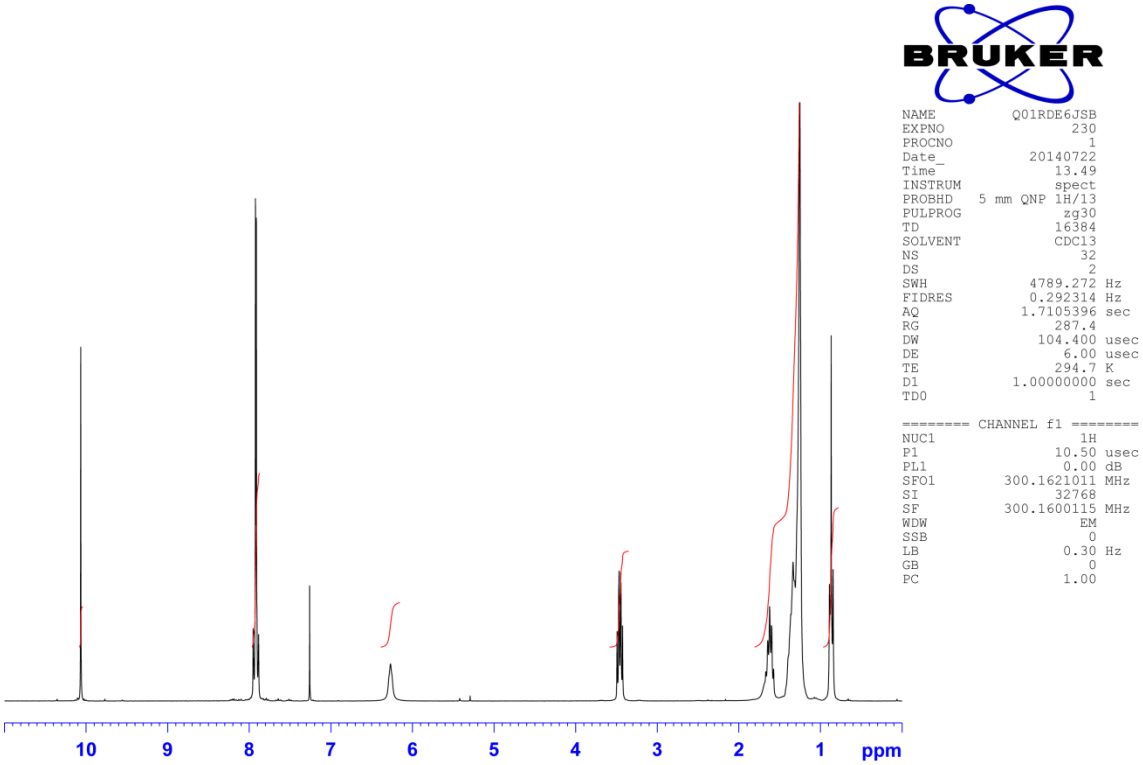

^{1}H NMR spectrum ($CDCl_3$, 300 MHz, 298 K) of compound **4a**.

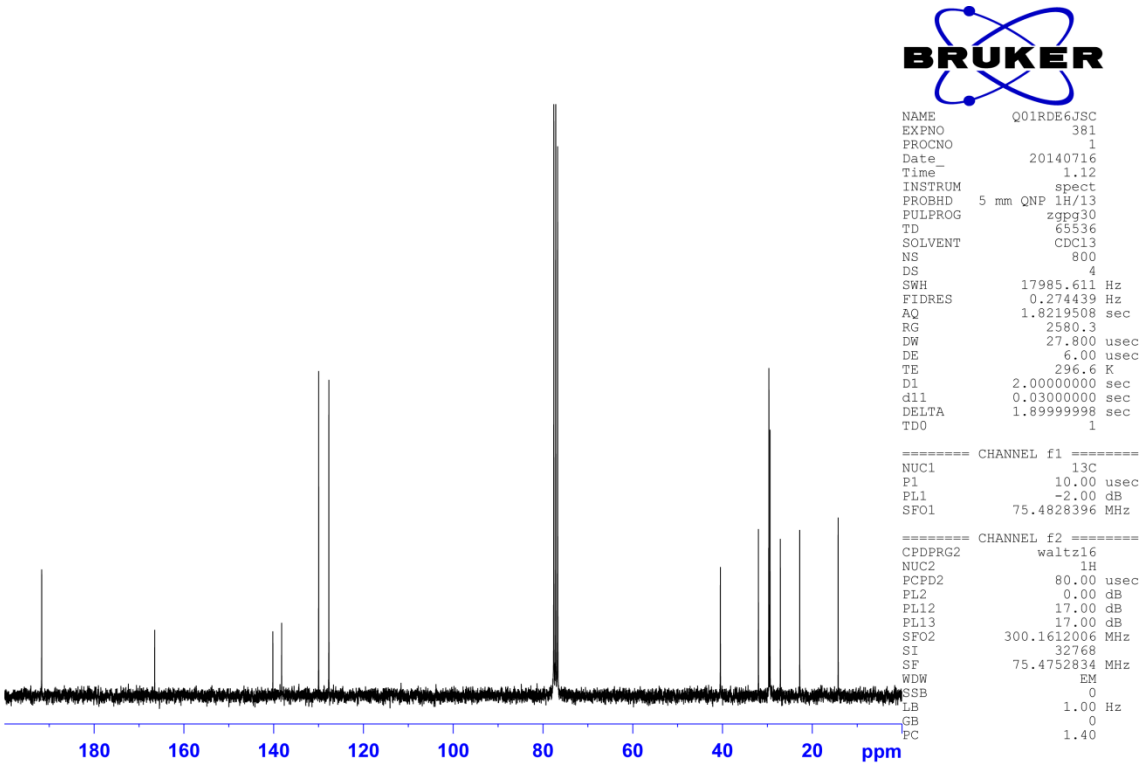

^{13}C NMR spectrum ($CDCl_3$, 75 MHz, 298 K) of compound **4a**.

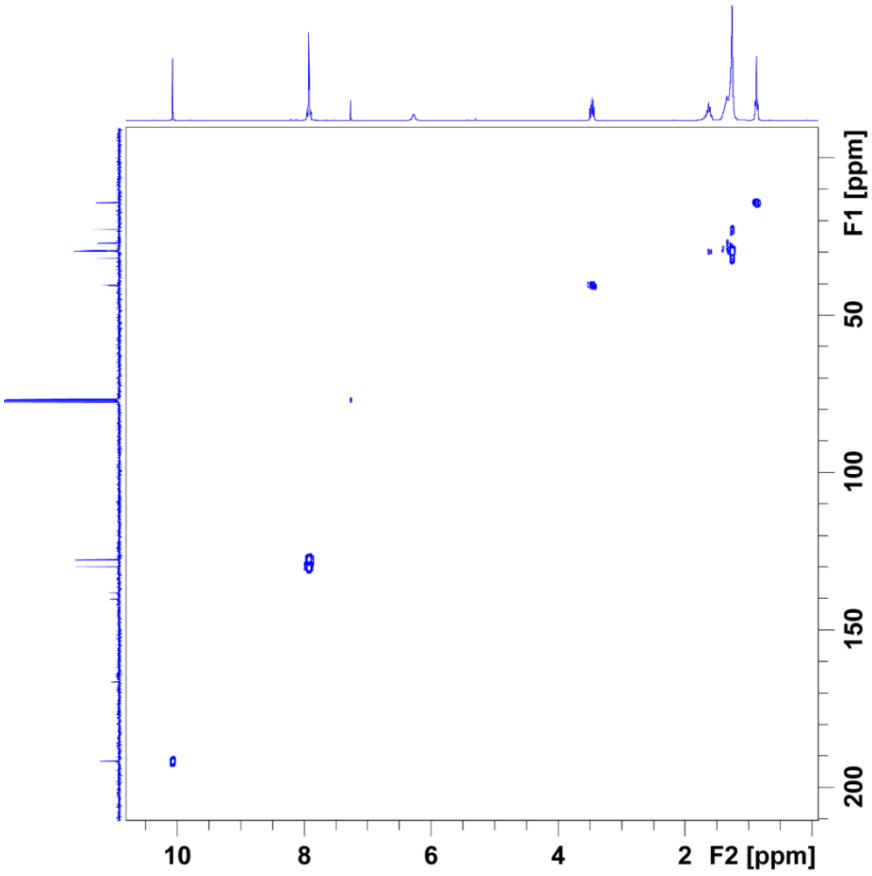

^{1}H, ^{13}C HMQC spectrum ($CDCl_3$, 298 K) of compound **4a**.

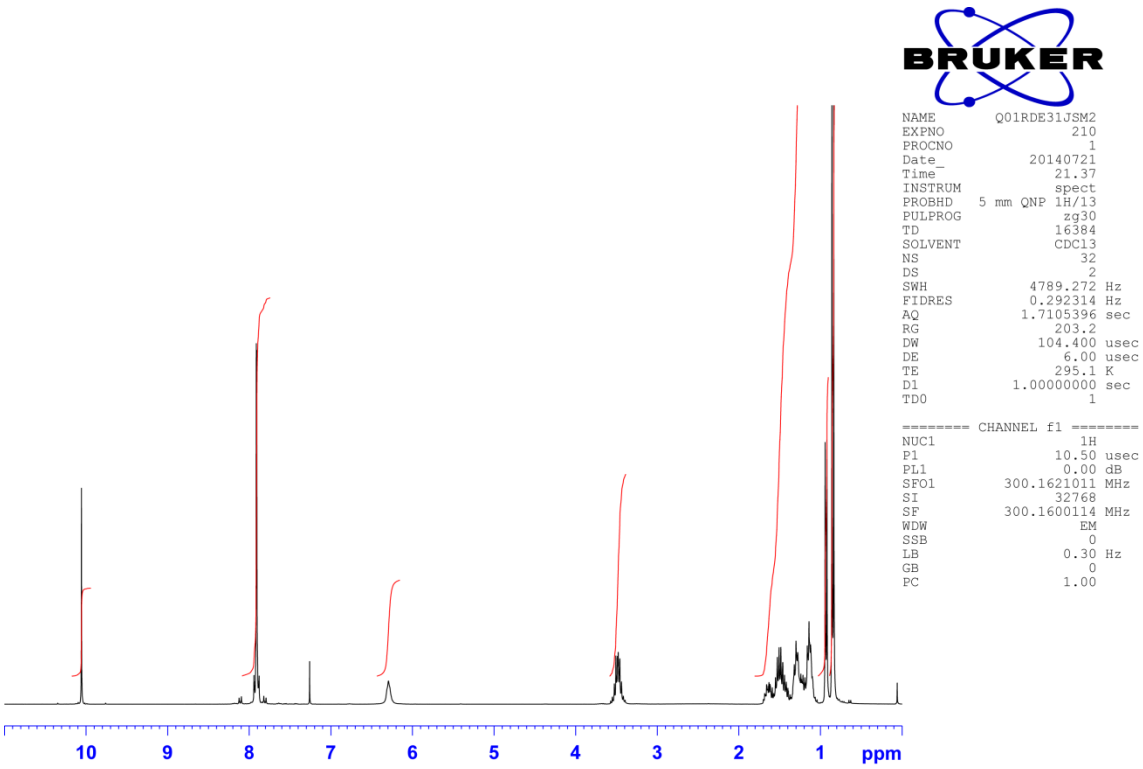

^{1}H NMR spectrum ($CDCl_3$, 300 MHz, 298 K) of compound **4b**.

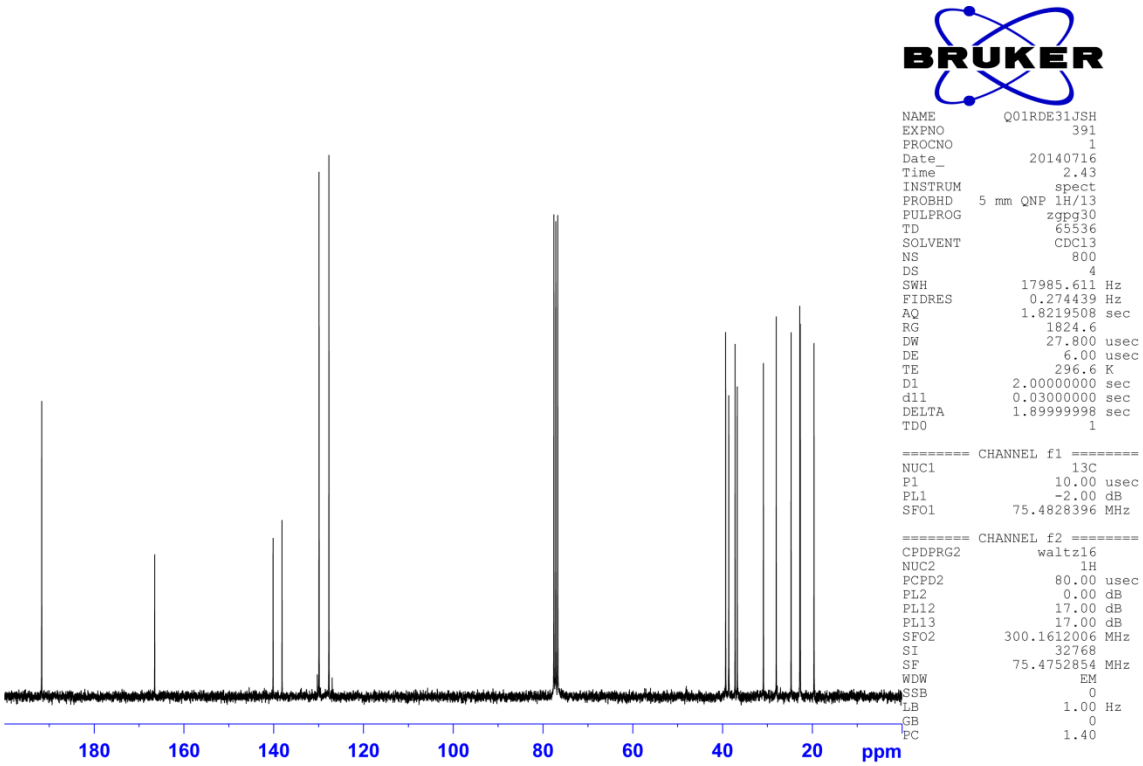

^{13}C NMR spectrum ($CDCl_3$, 75 MHz, 298 K) of compound **4b**.

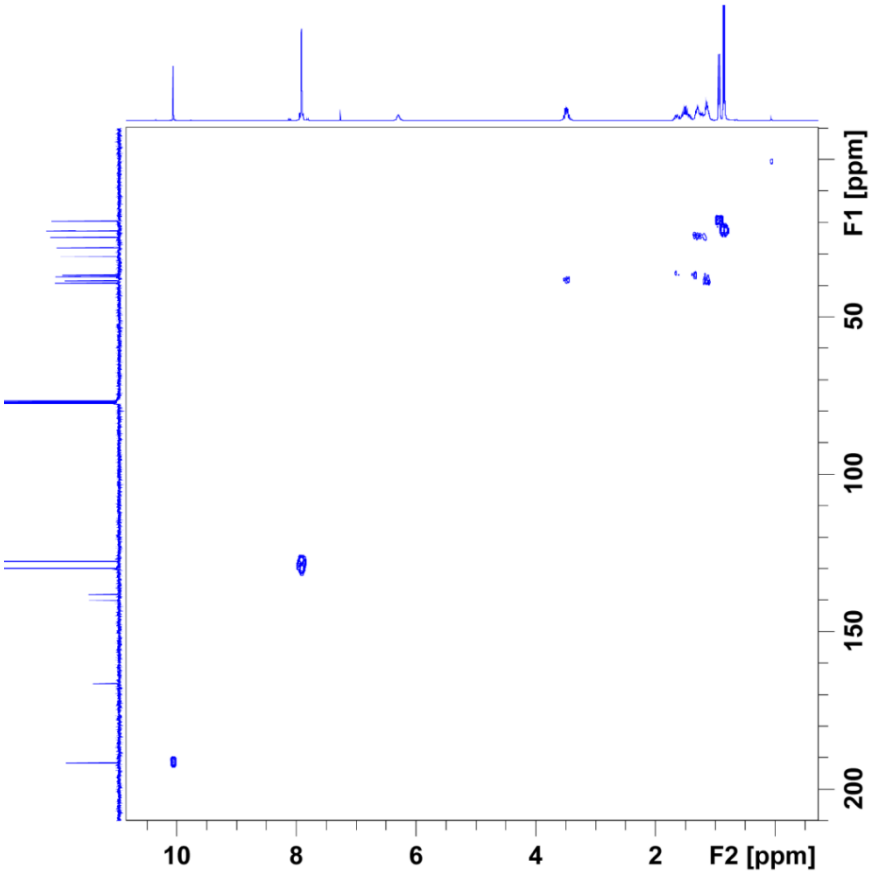

^{1}H, ^{13}C HMQC spectrum ($CDCl_3$, 298 K) of compound **4b**.

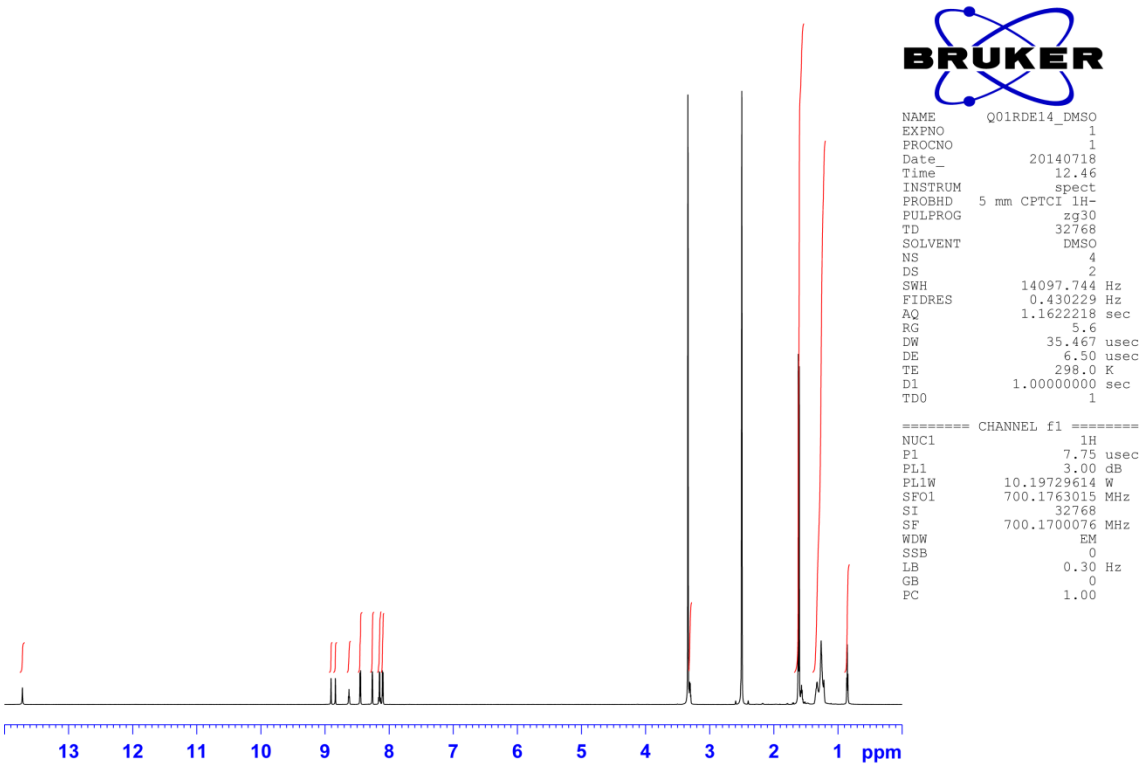

^{1}H NMR spectrum (DMSO, 700 MHz, 298 K) of compound **1**.

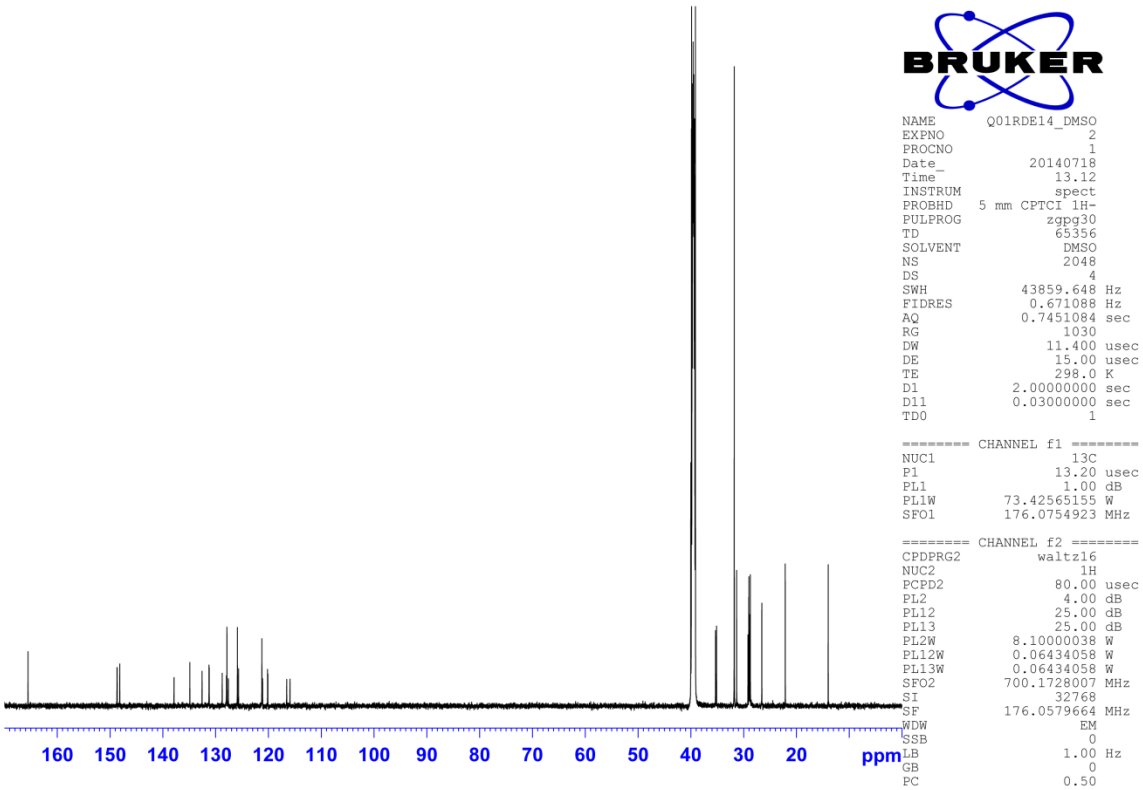

^{13}C NMR spectrum (DMSO, 176 MHz, 298 K) of compound **1**.

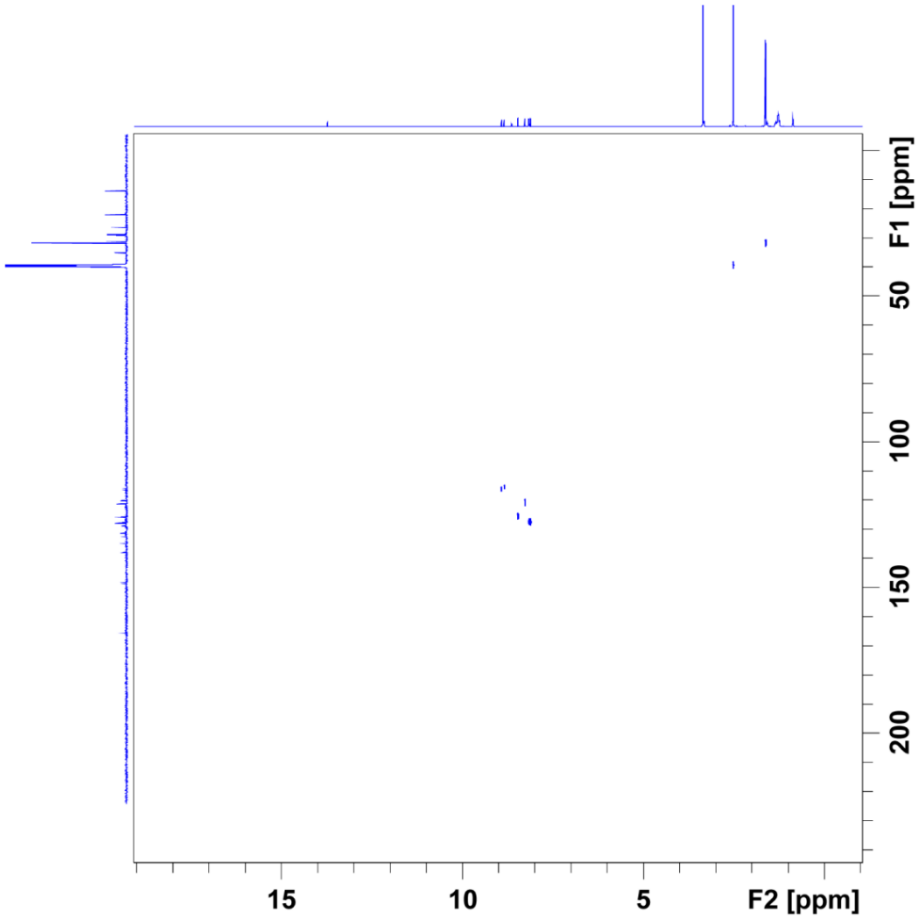

^{1}H, ^{13}C HSQC spectrum (DMSO, 298 K) of compound **1**.

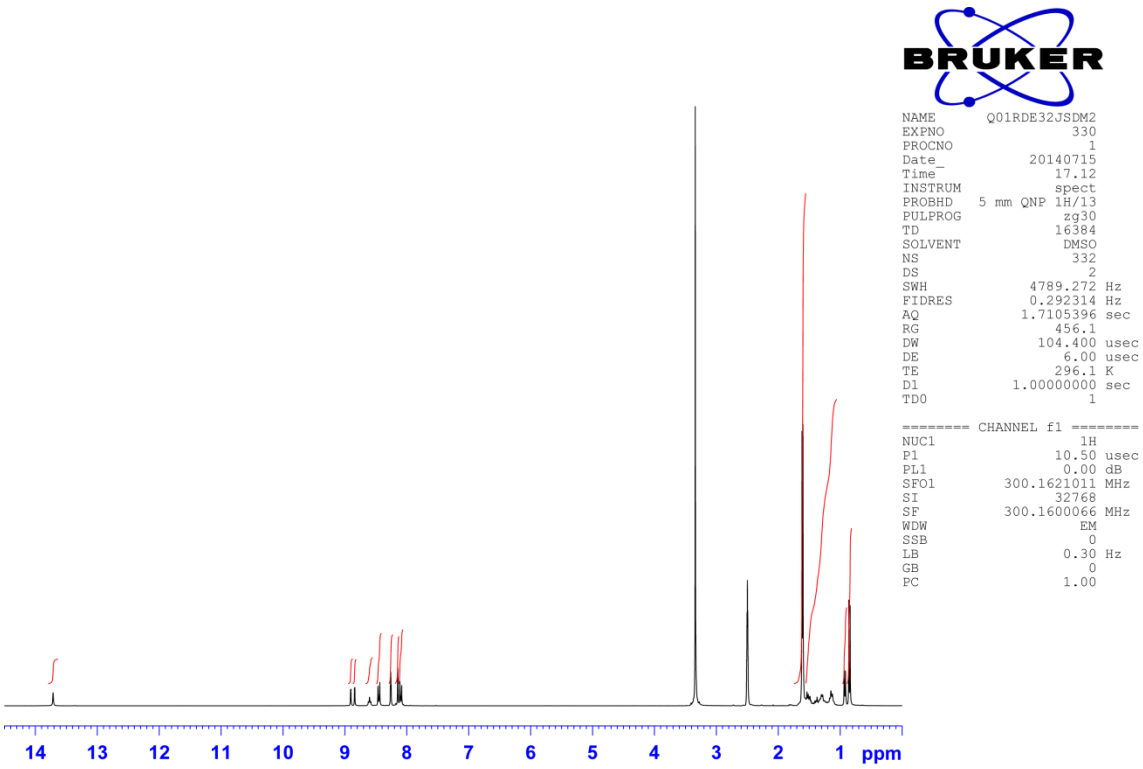

^{1}H NMR spectrum (DMSO, 300 MHz, 298 K) of compound **2**.

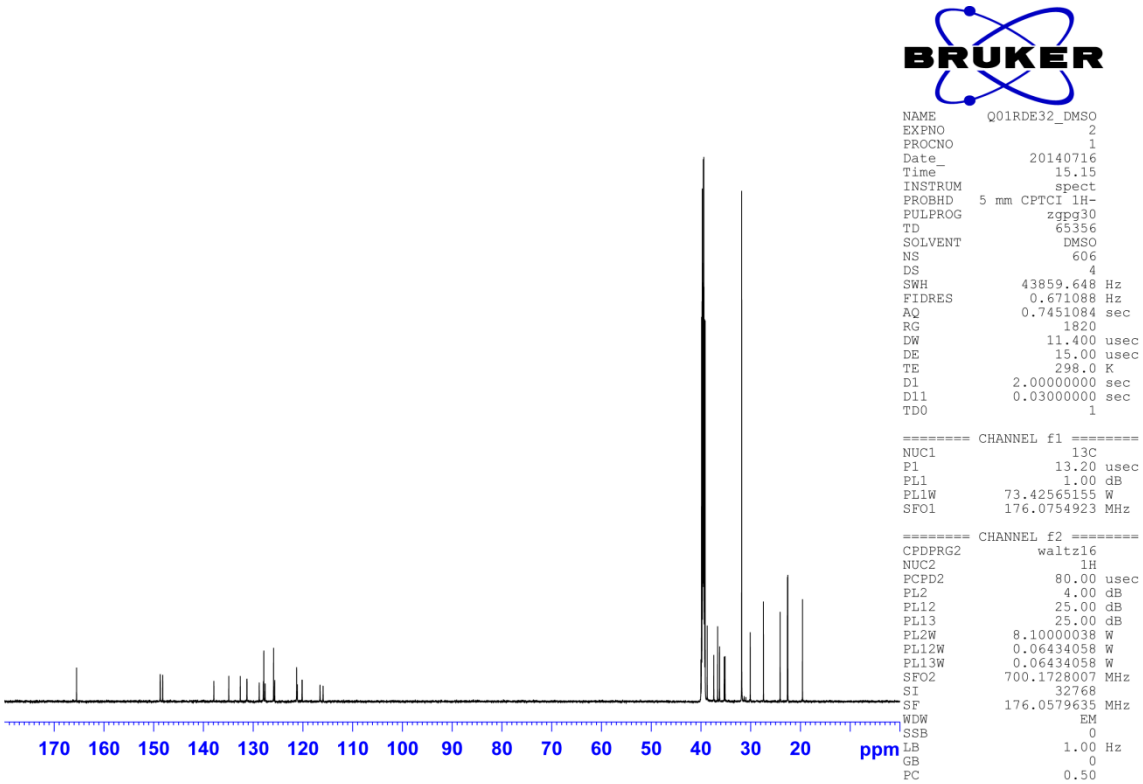

^{13}C NMR spectrum (DMSO, 176 MHz, 298 K) of compound **2**.

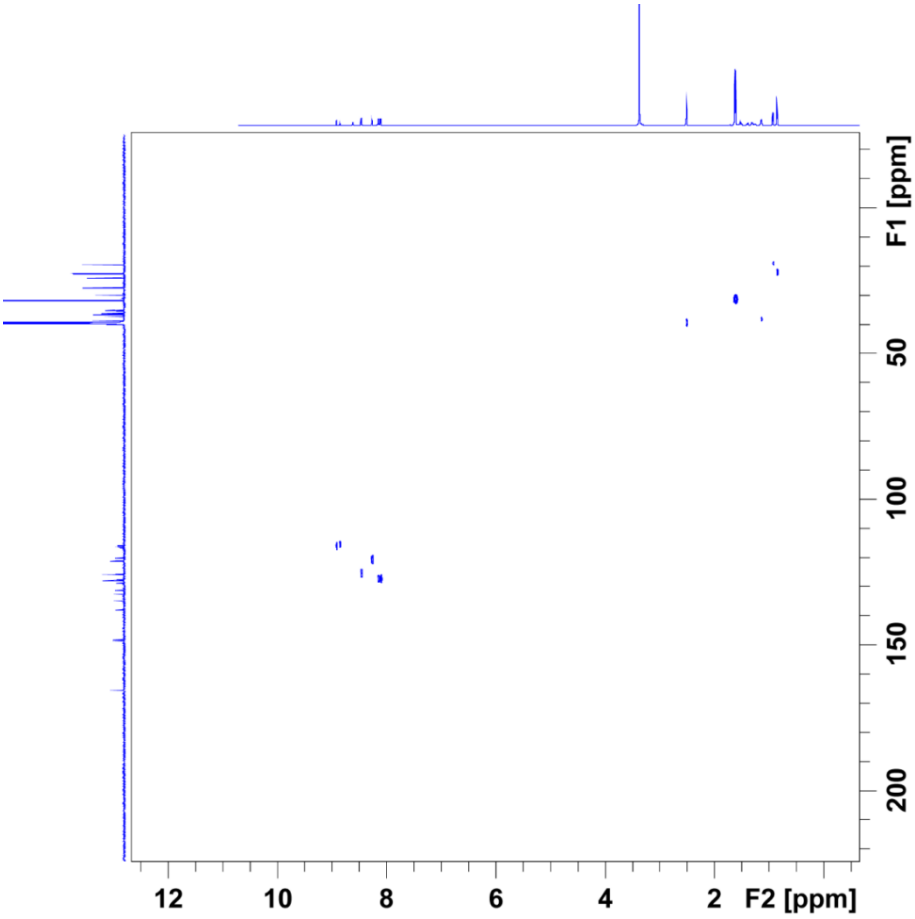

^{1}H, ^{13}C HSQC spectra (DMSO, 298 K) of compound **2**.

6. References

1 M. J. Frisch, G. W. Trucks, H. B. Schlegel, G. E. Scuseria, M. A. Robb, J. R. Cheeseman, G. Scalmani, V. Barone, B. Mennucci, G. A. Petersson, H. Nakatsuji, M. Caricato, X. Li, H. P. Hratchian, A. F. Izmaylov, J. Bloino, G. Zheng, J. L. Sonnenberg, M. Hada, M. Ehara, K. Toyota, R. Fukuda, J. Hasegawa, M. Ishida, T. Nakajima, Y. Honda, O. Kitao, H. Nakai, T. Vreven, J. A. Montgomery, J. E. Peralta, F. Ogliaro, M. Bearpark, J. J. Heyd, E. Brothers, K. N. Kudin, V. N. Staroverov, R. Kobayashi, J. Normand, K. Raghavachari, A. Rendell, J. C. Burant, S. S. Iyengar, J. Tomasi, M. Cossi, N. Rega, J. M. Millam, M. Klene, J. E. Knox, J. B. Cross, V. Bakken, C. Adamo, J. Jaramillo, R. Gomperts, R. E. Stratmann, O. Yazyev, A. J. Austin, R. Cammi, C. Pomelli, J. W. Ochterski, R. L. Martin, K. Morokuma, V. G. Zakrzewski, G. A. Voth, P. Salvador, J. J. Dannenberg, S. Dapprich, A. D. Daniels, Farkas, J. B. Foresman, J. V. Ortiz, J. Cioslowski and D. J. Fox, Gaussian 09, Revision D.01

2 S. Grimme, *J. Comput. Chem.*, 2006, **27**, 1787.

3 R. Ditchfield, W. J. Hehre and J. A. Pople, *J. Chem. Phys.*, 1971, **54**, 724.

4 M. M. Francl, W. J. Pietro, W. J. Hehre, J. S. Binkley, M. S. Gordon, D. J. Defrees and J. A. Pople, *J. Chem. Phys.*, 1982, **77**, 3654.

5 V. A. Rassolov, M. A. Ratner, J. A. Pople, P. C. Redfern and L. A. Curtiss, *J. Comput. Chem.*, 2001, **22**, 976.

6 A. D. Becke, *J. Chem. Phys.*, 1993, **98**, 5648.

7 S. Grimme, S. Ehrlich and L. Goerigk, *J. Comput. Chem.*, 2011, **32**, 1456.

8 H. Kruse and S. Grimme, *J. Chem. Phys.*, 2012, **136**, 154101.

9 J. Contreras-García, E. R. Johnson, S. Keinan, R. Chaudret, J.-P. Piquemal, D. N. Beratan and W. Yang, *J. Chem. Theory Comput.*, 2011, **7**, 625.

10 E. R. Johnson, S. Keinan, P. Mori-Sánchez, J. Contreras-García, A. J. Cohen and W. Yang, *J. Am. Chem. Soc.*, 2010, **132**, 6498.

11 G. A. Zhurko, ChemCraft 1.8 http://www.chemcraftprog.com

12 R. Dennington, T. Keith and J. Millam, GaussView, Version 5 *Semichem Inc*. Shawnee Mission, KS, 2009.

13 W. Humphrey, A. Dalke and K. Schulten, *J. Mol. Graphics*, 1996, **14**, 33.

14 T. Williams and C. Kelley, Gnuplot 4.6 http://gnuplot.info

15 M. Fontana, H. Chanzy, W. R. Caseri, P. Smith, A. P. H. J. Schenning, E. W. Meijer and F. Gröhn, *Chem. Mater.*, 2002, **14**, 1730.

16 J. Hu, D. Zhang and F. W. Harris, *J. Org. Chem.*, 2005, **70**, 707.